, , , , ,

Ba-substitution induced evolution of structural and magnetic properties of $La_{2-x}Ba_xCoIrO_6$ double perovskites

C. A. S. Vieira^a, B. J. Santos^b, J. G. Duque^b, E. M. Bittar^c, L. Bufaiçal^{a,*}

Abstract

The Iridium-based oxides are the subject of great recent interest due to the non-conventional physics that may emerge from the strong spin-orbit coupling present in 5d ions. Here, we explore the coupling between Ir and Co in the $\text{La}_{2-x}\text{Ba}_x\text{CoIrO6}$ perovskites $(x=0,\,0.5,\,0.75\text{ and }1.0)$, where the structural, electronic, and magnetic properties of the series are investigated by means of x-ray powder diffraction and magnetometry. The system's crystal structure evolves from the monoclinic P21/n to the triclinic $I\bar{1}$ space group as the Ba concentration increases. Measurements of magnetization revealed ferrimagnetic behavior in $x=0,\,0.5$ and 0.75 compounds, possibly resulting from antiferromagnetic coupling between $\text{Co}^{2+/3+}$ and Ir^{4+} . In contrast, for x=1.0 a clear collinear antiferromagnetic character is observed for the Co^{2+} ions, resulting from the quenching of the Ir^{5+} magnetic moment. The evolution of the magnetic properties of the series is discussed in terms of the structural and electronic changes, as well as the spin-orbit coupling in Ir.

Keywords: Iridium; Cobalt; Spin-orbit coupling; Double-perovskite

1. Introduction

The strong spin-orbit coupling (SOC) underlying the physics of 5d-based oxides can lead to a variety of exotic phenomena. For iridates specifically, the interplay between SOC, electron correlation, and crystal field effects creates a rich landscape for unconventional quantum states, such as topological Mott insulators [1], Weyl semimetals [2], spin-liquid candidates [3], and Kitaev materials [4]. Among these, double perovskites (DP) with the general formula $A_2BB'O_6$

 $Email\ address: \ {\tt lbufaical@ufg.br}\ (L.\ Bufaical)$

^a Instituto de Física, Universidade Federal de Goiás, 74001-970, Goiânia, GO, Brazil
^b Programa de Pós-Graduação em Física, Campus Prof. José Aluísio de Campos, UFS, 49100-000 São Cristóvão, SE, Brazil

^c Centro Brasileiro de Pesquisas Físicas, Rua Dr. Xavier Sigaud 150, 22290-180, Rio de Janeiro, RJ, Brazil

^{*}Corresponding author

provide a feasible framework to modulate magnetic interactions through chemical substitution, due to the structure's flexibility to accommodate various rareearth and alkaline-earth ions at the A site, and transition-metal (TM) ions at the B/B' sites [5, 6, 7].

Particularly, 3d-5d DPs, where a 3d magnetic ion couples with a 5d ion with strong SOC, have attracted attention due to their interesting magnetic ground states [8, 9]. La₂CoIrO₆ is a paradigmatic example of a 3d-5d DP, on which the antiferromagnetic (AFM) coupling between Co²⁺ (3d⁷) and Ir⁴⁺ (5d⁵) leads to a ferrimagnetic (FIM) and insulating system that undergoes magnetodielectric effect below T_C [10]. When La³⁺ is partially replaced by Ca²⁺, the changes imposed in the Co/Ir oxidation states leads to competing magnetic interactions that result in spin-glass behavior [11]. The similar ionic radii of Ca²⁺ and La³⁺ in XII coordination (1.34 and 1.36 Å, respectively) [12] leads to minimal structural changes with doping in this series, with the monoclinic $P2_1/n$ space group being maintained along the whole series [13]. Therefore, the magnetic evolution of the La_{2-x}Ca_xCoIrO₆ system may be primarily associated with the electronic changes.

For Sr^{2+} substitution at the La^{3+} site in $\mathrm{La}_{2-x}\mathrm{Sr}_x\mathrm{CoIrO}_6$, a non-collinear magnetic structure is observed that is dramatically affected by the Sr content [14, 15]. In this case, albeit the impact of Sr^{2+} in the crystal structure is higher than that of Ca^{2+} due to the former's larger ionic radius (1.44 Åin XII coordination [12]), the $P2_1/n$ symmetry is preserved up to 50% of substitution. To access more pronounced crystallographic changes, the use of even more discrepant elements at the A-site is necessary.

In this context, Ba-doping in the La-site provides an effective way to induce structural changes due to the large ionic radius of $\mathrm{Ba^{2+}}$ (1.61 in XII coordination [12]). Furthermore, Ba-doping changes the valence state balance, potentially altering the oxidation states of Co and Ir ions, thus affecting the magnetic interactions. In this work, we systematically study the structural, electronic, and magnetic evolution of $\mathrm{La_{2-x}Ba_{x}CoIrO_{6}}$ (x=0,0.5,0.75,1.0) perovskites. By employing x-ray powder diffraction (XRD) and magnetization measurements, we explore how Ba-substitution influences the crystal structure, electronic configuration, and magnetic ground state of this series. The observed phenomena are discussed in terms of lattice distortions, valence state modifications, and the pivotal role of SOC in modulating the magnetic properties of these compounds.

2. Experimental Methods

The polycrystalline samples of the $\text{La}_{2-x}\text{Ba}_x\text{CoIrO}_6$ series (x=0, 0.5, 0.75 and 1.0) here investigated were synthesized by conventional solid-state reaction, in an air atmosphere. Stoichiometric amounts of La_2O_3 (purity $\geq 99.9\%$), BaCO_3 (purity $\geq 99\%$), Co_3O_4 (purity $\geq 99.5\%$) and metallic Ir in powder form (purity $\geq 99.9\%$), all from Sigma Aldrich, were mixed and heated at 900°C for 24 hours in an air atmosphere. Later, the samples were re-grinded before a second step at 1100°C for 48 hours. Finally, each material was grinded, pressed

into pellets, and heated at 1200° C for an additional 24 hours. Attempts to produce the x=0.25 concentration using the same synthesis route did not succeed, resulting in the formation of impurity phases.

X-ray powder diffraction (XRD) data were collected at room temperature using a Cu K_{α} radiation operating at 40 kV and 40 mA at Centro Brasileiro de Pesquisas Físicas (CBPF), Brazil. The XRD data was carried over the angular range of $10^{\circ} \leq 2\theta \leq 90^{\circ}$, with a 2θ step size of 0.01°. Rietveld refinement was performed using GSAS software and its graphical interface program [16]. The refinements were conducted assuming a Pseudo-Voigt function for the peak-profiles, and a 8-terms shifted Chebyschev function for the background. The La/Ba isotropic atomic displacement parameters (U_{iso}) and atomic positions were constrained to be the same, as well as the U_{iso} of the oxygen ions, in order to avoid divergence during the refinements.

The dc magnetic measurements were carried out using a Quantum Design PPMS magnetometer at CBPF. Magnetization as a function of temperature [M(T)] measurements were performed in both zero-field-cooled (ZFC) and field-cooled (FC) modes. Magnetization as a function of applied magnetic field [M(H)] curves were carried out after the ZFC protocol.

3. Results and Discussion

Fig. 1(a) shows the Rietveld refinement fitting of the XRD pattern of the x = 1.0 sample as a representative of the whole series, for which similar reliability factors were achieved, as depicted in Table 1. The Rietveld refinement fittings of the other samples here investigated are depicted in the Supplementary Material, together with the atomic coordinates and other information regarding the crystal structures.

In agreement with previous reports, the crystal structures of both x=0 and 0.5 could be well refined within the monoclinic $P2_1/n$ space group [10, 11, 17], signaling that a 25% Ba substitution at the La site is insufficient to induce a structural transition. For x=1.0, however, attempts to refine the crystal structure in this same monoclinic symmetry did not succeed. Instead, a good match was achieved with the triclinic $I\bar{1}$ space group. The inset of Fig. 1(a) compares stretches of the x=0.5 and 1.0 patterns, endorsing the structural transition. For x=0.75 the crystal structure could not be well refined when a single phase belonging to $P2_1/n$ or to $I\bar{1}$ space group was considered individually. But a good match was achieved when both space groups were considered simultaneously. The refinement indicated about 60% and 40% in mass of the $P2_1/n$ and $I\bar{1}$ phases, respectively, therefore evidencing that this sample represents an intermediate case between the x=0.5 and 1.0 compounds.

Fig. 1(b) compares selected Bragg reflections for the samples of interest, where a systematic shift toward smaller 2θ angles with increasing Ba content is evidenced. As depicted in the inset, this reflects the increase in the unit cell volume (V), related to the fact that the Ba²⁺ ionic radius is significantly larger than that of La³⁺ (respectively 1.61 and 1.36 Å, in XII coordination) [12]. It should be noted that the V expansion is remarkably larger from x = 0.5 to 1.0

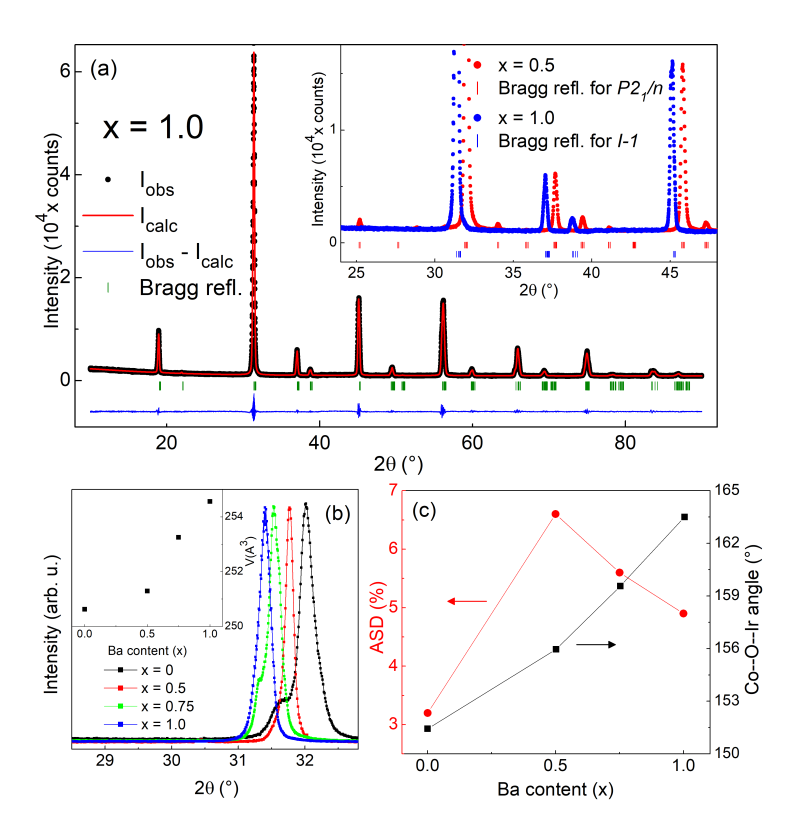


Figure 1: (a) Rietveld refinement fitting of the x=1.0 crystal structure from XRD. The inset compares the XRD patterns of the x=0.5 and 1.0 samples, where the vertical lines represent the Bragg reflections for the $P2_1/n$ and $I\overline{1}$ space groups, highlighting the distinct diffraction peaks. (b) Main diffraction peaks for x=0, 0.5, 0.75 and 1.0, where the inset shows the evolution of the unit cell volume. (c) Co/Ir ASD and \langle Co-O-Ir \rangle bond angle as a function of Ba content.

Table 1: Main lattice parameters and reliability factors obtained from the Rietveld refinements. The numbers in parentheses represents the standard uncertainties in the last digits.

Sample (x)	0	0.5	0.75	0.75	1.0				
\overline{SG}	$P2_1/n$	$P2_1/n$	$P2_1/n (60\%)$	$I\overline{1} \ (40\%)$	$I\overline{1}$				
a (Å)	5.57789(16)	5.63357(14)	5.61075(9)	5.63202(7)	5.65156(8)				
b (Å)	5.67845(15)	5.61535(14)	5.66650(10)	5.63058(9)	5.63271(10)				
c (Å)	7.91281(19)	7.94361(21)	7.96309(8)	7.99013(13)	7.99710(10)				
$V(\mathring{A}^3)$	250.629(14)	251.292(5)	253.172(9)	253.360(5)	254.568(8)				
α (°)	90	90	90	89.708(1)	89.631(2)				
β (°)	89.956(5)	90.036(4)	89.852(1)	90.508(1)	90.280(2)				
γ (°)	90	90	90	90.390(1)	90.061(2)				
ASD(%)	4.4	7.5	4.9	6.6	4.9				
$\langle \text{Co-O} \rangle \text{ (Å)}$	2.0088(12)	2.0090(11)	2.0152(6)	2.0049(7)	1.9931(13)				
$\langle \text{Ir-O} \rangle \text{ (Å)}$	2.0959(12)	2.0555(11)	2.0388(6)	2.0498(7)	2.0449(13)				
$\langle \text{Co-O-Ir} \rangle \ (^{\circ})$	151.456(17)	155.946(16)	159.069(12)	160.318(13)	163.503(16)				
R_{wp} (%)	6.3	4.9	4.2	4.2	4.7				
R_p (%)	4.8	3.5	3.2	3.2	3.7				
		·	· ·	·					

than from x=0 to 0.5. This is most likely related to the prominent decrease of the average B-site radius from x=0 to 0.5 since, as will be discussed in the context of the magnetic properties, the 25% $\mathrm{Ba^{2+}}$ for $\mathrm{La^{3+}}$ substitution primarily increases the Co formal valence from $\mathrm{Co^{2+}}$ to $\mathrm{Co^{2.5+}}$ (the $\mathrm{Co^{2+}}$ and $\mathrm{Co^{3+}}$ radii are respectively 0.745 and 0.61 Å, in high spin state) [12]. On the other hand, for further Ba-doping there is a tendency to return to the $\mathrm{Co^{2+}}$ configuration, while Ir valence tends to increase ($\mathrm{Ir^{4+}}$ and $\mathrm{Ir^{5+}}$ radii are 0.625 and 0.57 Å, respectively) [12]. The V expansion with increasing Ba content is also manifested in the increase of the average Co-O-Ir bond angle, Fig. 1(c). This was expected, since the B-O-B' angles usually increase with V in DPs [6, 7].

Importantly, the anti-site disorder (ASD) at the Co and Ir sites, extracted from the Rietveld refinements, does not evolve monotonically. As Fig. 1(c) shows, it initially increases from x=0 to 0.5, followed by a systematic decrease for larger Ba-doping. The ASD is known to be ruled by the differences between the B/B' charges and ionic radii, as well as by the unit cell volume [18]. Therefore, the changes observed for the ASD are, again, directly related to the evolution of the crystal structure and the Co/Ir electronic configurations. For x=0, one has mainly $\mathrm{Co^{2+}}$ and $\mathrm{Ir^{4+}}$, whose charges and radii differ significantly [11]. Thus, a relatively small ASD is noticed. For x=0.5, as will be discussed in the context of magnetic properties, the introduction of $\mathrm{Ba^{2+}}$ at the $\mathrm{La^{3+}}$ site most likely acts to increase the Co valence state, while Ir remains nearly tetravalent. The presence of 50% of $\mathrm{Co^{3+}}$ makes the charges and radii of the transition metals (TM) more alike. Furthermore, the V expansion facilitates the permutation between the TMs, resulting in a pronounced increase in the ASD. On the other hand, for Ba-doping larger than 25% there is a tendency to return

to $\mathrm{Co^{2+}}$ while the Ir valence increases, resulting in larger differences between the $\mathrm{Co/Ir}$ charges and radii that lead to the decrement the ASD. However, V systematically enhances with Ba-content. From these joint effects it results that, although the ASD decreases from x=0.5 to 1.0, it does not achieve the same small value as that found for x=0. As we shall see next, the structural changes observed along the series directly impact the system's magnetic properties.

The ZFC-FC M(T) measurements, performed with a magnetic field H =0.1 T, are depicted in Fig. 2. The FC curves of x=0 and 0.5 are typical of ferromagnetic (FM) or FIM compounds. The magnitudes of the magnetization at low temperatures, however, are much smaller than expected for a FM, indicating a FIM character that results from antiferromagnetic (AFM) coupling between Co and Ir. The magnetic ordering temperature of x = 0, $T_C \simeq 94$ K, agrees with previous reports, being associated with the onset of AFM coupling between Co^{2+} and Ir^{4+} [10, 13]. For x = 0.5, T_C decreases to approximately 70 K. It must be noticed that the magnitude of the magnetization is also reduced when compared with the pristine compound. Similar behavior was observed in the $La_{2-x}Ca_xCoIrO_6$ and $La_{2-x}Sr_xCoIrO_6$ series, for which the magnetization progressively decreases with increasing the content of alkaline-earth ion [11, 14]. Here, such evolution must be related to changes in the magnetic structure and/or to the increased ASD at x = 0.5 that hampers the percolation of exchange interactions due to the increased presence of competing magnetic phases and frustration.

For x=0.75 and 1.0, however, the dramatic reduction of the magnetization cannot be accounted for by the ASD. The inset of Fig. 2(b) shows magnified views of the M(T) curves for these compounds, where a cusp typical of AFM systems is noticed at $T_N \simeq 61$ K for x=1.0, followed by a broader peak at ~ 25 K. The low temperature anomaly is possibly related to the onset of glassy magnetic behavior, or to the presence of short-range Co-Co/Ir-Ir couplings brought by the ASD. In the latter case, the short-range correlations may be also present in the x=0 and 0.5 compounds, but they would be masked by the magnetization from the major FIM coupling. The use of additional techniques, such as AC magnetic susceptibility, is necessary to unravel this issue. Interestingly, the ZFC curve for x=0.75 seems to present both characteristics of FIM and AFM couplings. It shows a magnetic transition similar to that of FM/FIM compounds at ~ 66 K followed by a cusp similar to that of AFM systems at ~ 26 K. Details about the magnetic properties of this compound will be addressed below

The fits of the reciprocal magnetic susceptibility (χ^{-1}) curves with the Curie-Weiss (CW) law are displayed in Fig. 2(c). For x=0, this yields a CW temperature $\theta_{CW}=-53$ K and an effective magnetic moment $\mu_{eff}=5.0~\mu_B/{\rm f.u.}$. The negative θ_{CW} confirms the predominance of AFM coupling, corroborating the FIM scenario. The experimental effective moment can be compared with the expected value calculated with the equation usually adopted for systems presenting two or more magnetic ions

$$\mu_{calc} = \sqrt{\mu_1^2 + \mu_2^2 + \mu_3^2 \dots} \tag{1}$$

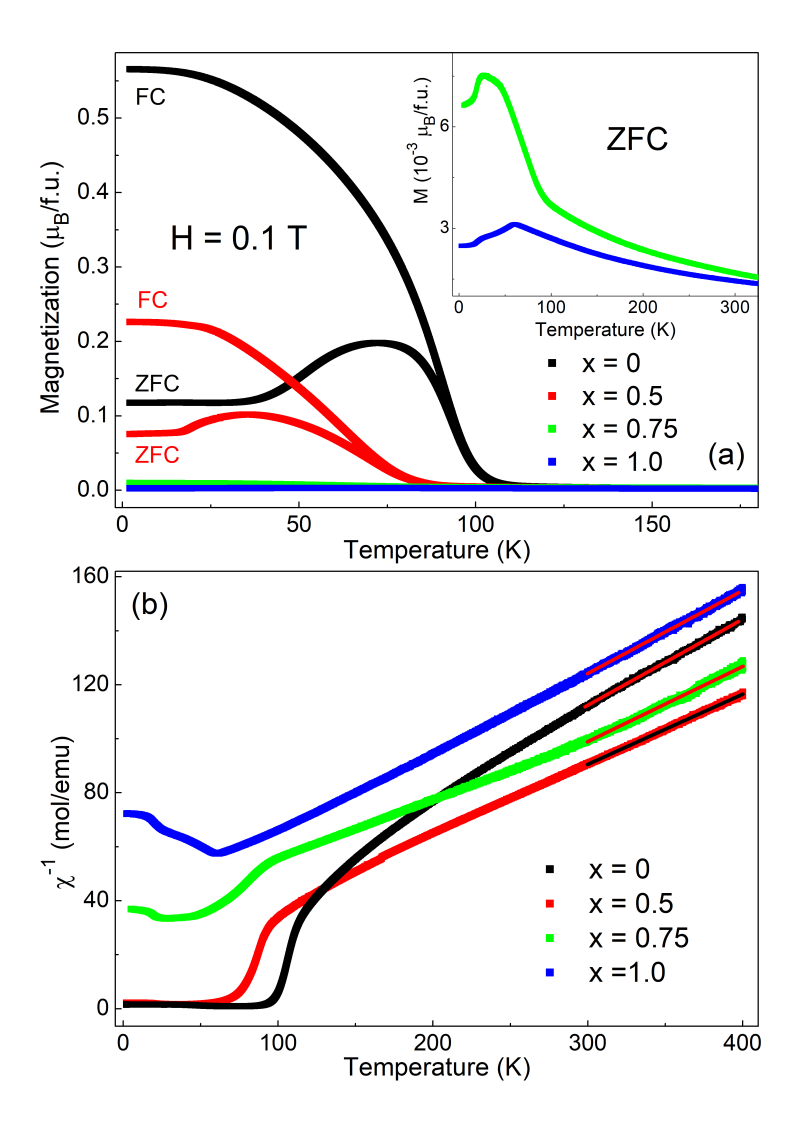


Figure 2: (a) ZFC-FC M(T) curves measured with H=0.1 T. The inset shows a magnified view of the low temperature region of x=1.0, highlighting its T_N . (b) χ^{-1} curves, where the straight lines represent the best fits with the CW law.

Table 2: Main results obtained from the M(T) and M(H) curves.

$\overline{\text{Sample }(x)}$	0	0.5	0.75	1.0
T_C/T_N (K)	94	70	66	61
θ_{CW} (K)	-53	-48	-56	-104
$\mu_{eff}~(\mu_B/{ m f.u.})$	5.0	5.5	5.3	5.1
$\mu_{calc}~(\mu_B/{ m f.u.})$	5.1	5.4	5.3	4.8
H_C (T)	1.8	1.9	0.15	-
$M_R \; (\mu_B/{ m f.u.})$	0.669	0.253	0.007	-

Assuming the standard individual moments of Co²⁺ ($\mu_{Co^{2+}} = 4.8 \ \mu_B$) and Ir⁴⁺ ($\mu_{Ir^{4+}} = 1.7 \ \mu_B$) [19], one obtains $\mu_{calc} = 5.1 \ \mu_B/\text{f.u.}$, fairly close to the experiment.

For x=0.5, the CW fit yields $\theta_{CW}=-48$ K and $\mu_{eff}=5.5~\mu_B/{\rm f.u.}$. The enhancement of μ_{eff} with respect to x=0 gives further evidence that the the 25% of Ba²⁺ to La³⁺ substitution leads to the increase of the Co oxidation state to Co^{2.5+}. If, instead, Ir valence would been enhanced to +4.5 one should expect the decrease of μ_{eff} , since it is known that the large SOC further lifts the degeneracy of the t_{2g} orbitals in this 5d ion, in a way that Ir⁵⁺ is expected to have a zero net magnetic moment [11, 20, 21, 22, 23]. Here we remind that this scenario is endorsed by the increased ASD, caused by the greater similarity between the Co/Ir valences and radii. Adopting the standard moments for Co²⁺, Ir⁴⁺ and Co³⁺ ($\mu_{Co^{3+}}=5.4~\mu_B$) [19] in Eq. 1, we get $\mu_{calc}=5.4~\mu_B$ /f.u., also close to the experimental value.

For x=0.75, the CW fit yields $\theta_{CW}=$ -56 K, while μ_{eff} decreases to 5.3 $\mu_B/{\rm f.u.}$. Such a decrease of μ_{eff} with respect to the value found for x=0.5 cannot be explained by a further increase in the Co valence, otherwise the effective moment would increase. Instead, the increase of the Ir oxidation state is most likely, also agreeing with the decreased ASD. Assuming in Eq. 1 that the further Ba-doping leads to ${\rm Ir}^{4.25+}$ configuration, while the ${\rm Co}^{2.5+}$ formal valence remains unchanged, we have $\mu_{calc}=5.3~\mu_B/{\rm f.u.}$, matching with the experimentally observed decrease of μ_{eff} .

For x=1.0, the effective moment further reduces to 5.1 $\mu_B/{\rm f.u.}$. Two possible scenarios can be invoked to account for this: (i) the Ir oxidation states increases to +4.5 while the ${\rm Co^{2.5+}}$ mixed valence is maintained; (ii) Ir is fully oxidized to pentavalent state while Co is reduced to the bivalent state. Eq. 1 yields respectively $\mu_{calc}=5.2$ and $4.8~\mu_B/{\rm f.u.}$ for (i) and (ii), matching with the decrease of μ_{eff} experimentally observed. Although the paramagnetic moment calculated within picture (i) is closer to the experiment, we believe that the later scenario is most likely, since the stabilization of ${\rm Ir^{5+}}$ have been confirmed for several LaABIrO₆ (A = Ca, Sr, Ba; B = 3d TM ions) perovskites [11, 22, 26, 27, 28]. Furthermore, the line-shape of the M(T) curves observed for this sample are characteristic of a pure AFM system, i.e. typical of a single magnetic ion, whereas a FM- or FIM-like curve should be expected for a system presenting two or more magnetic ions. Here, the difference between the calculated and

experimental moments could be due to a significant orbital contribution to the Co moment resulting from a weak crystal field, as suggested by the large unit cell volume [10, 11, 24]. In any case, the possible presence of small amounts of $\mathrm{Co^{3+}/Ir^{4+}}$ cannot be ruled out.

Regarding the overall results of the CW fits, the θ_{CW} values obtained differ from the T_C/T_N observed. Despite the linear character of the curves in the PM region of the χ^{-1} plots and the correspondingly good fits achieved, the discrepancies could be related to deviations from Curie-Weiss (CW) behavior, as previously reported for similar Ir-based DPs [25, 26, 27]. Nevertheless, the negative θ_{CW} values obtained for all compounds endorse the scenario of AFM coupling between Co and Ir in x=0,0.5 and 0.75, and between the Co moments in x=1.0.

The M(H) curves are depicted in Fig. 3. The loops of x=0 and 0.5 are typical of FM or FIM polycrystals, with an S-shaped form, large remanent magnetizations (M_R) and coercive fields (H_C) of the order of 2 T. But again, the magnetization values are much smaller than expected for FM coupling between Co and Ir. Furthermore, the magnetization does not saturate even at H=9 T, continuing to increase linearly at high fields. These features further suggest a FIM character resulting from AFM coupling between Co and Ir. The decreased magnetization of x=0.5 with respect to x=0 may be related to the increased ASD in the former compound. Indeed, the larger slope of the x=0.5 curve at high fields suggests an augmented contribution of short-range AFM couplings and/or paramagnetic (PM) contributions brought by the ASD. Alternatively, the magnetic evolution observed from x=0 to 0.5 could be related to changes in presumably non-collinear spin superstructures of Co and Ir sites, as suggested for $\text{La}_{2-x}\text{Sr}_x\text{CoIrO}_6$ [14].

The M(H) curve of x=0.75 lacks the S-shaped form, and the magnetization is significantly reduced with respect to that of x=0 and 0.5. But non-negligible H_C and M_R are observed, suggesting the presence of FIM coupling. For x=1.0, however, the M(H) curve is typical of AFM systems, exhibiting negligible M_R and H_C . This endorses the scenario of a purely AFM ordering on the Co superstructure for this compound, due to the zero net magnetic moment of ${\rm Ir}^{5+}$ caused by its strong SOC that lifts the t_{2g} degeneracy of this $5d^4$ ion into a fully occupied $j_{3/2}$ quadruplet and an empty $j_{1/2}$ doublet. Interestingly, both the M(T) and M(H) curves of LaBaCoIrO₆ are distinct from the FM-like shapes observed in LaSrCoIrO₆ and LaCaCoIrO₆ [14, 27]. Albeit the ${\rm Co}^{2+}$ and non-magnetic ${\rm Ir}^{5+}$ configurations also dominate the latter compounds, the more distorted crystal structures lead to spin canting on the Co moments. In contrast, for the more symmetric LaBaCoIrO₆ system, a collinear AFM superstructure is most likely.

4. Conclusions

We have investigated the structural, electronic, and magnetic properties of $\text{La}_{2-x}\text{Ba}_x\text{CoIrO}_6$ double perovskites ($x=0,\,0.5,\,0.75,\,1.0$). Our results reveal a progressive structural evolution from monoclinic to triclinic symmetry upon

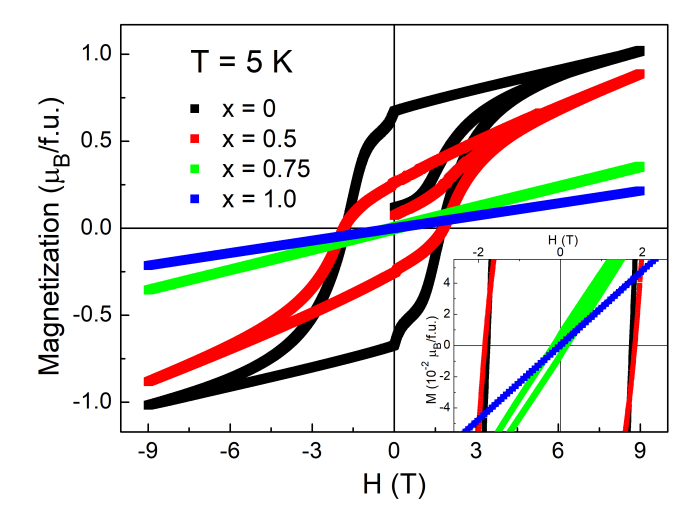


Figure 3: M(H) curves measured at 5 K. The inset shows a magnified view of the low field region.

Ba-doping, accompanied by a suppression of ferrimagnetic order. The anti-site disorder at the Co/Ir sites increases from x=0 to x=0.5, this behavior being consistent with the initial increase of the Co oxidation state up to 25% Ba²⁺ substitution at the La³⁺ site. In contrast, further Ba-doping seems to increase the Ir valence, with this ion reaching the pentavalent state while Co returns to a bivalent configuration for x=1.0. The structural and electronic evolution explain the changes in the magnetic properties of the series and further support the scenario of large SOC on Ir, where the x=0, 0.5 and 0.75 samples exhibit FIM behavior resulting from AFM coupling between $\text{Co}^{2+/3+}$ and Ir^{4+} , while for x=1.0 the presence of non-magnetic Ir^{5+} leads to a typically collinear AFM character at the Co^{2+} superstructure.

Acknowledgements

This work was supported by the Brazilian funding agencies: Fundação de Amparo à Pesquisa do Estado de Goiás (FAPEG) [No. AUX2024301000048], Fundação Carlos Chagas Filho de Amparo à Pesquisa do Estado do Rio de Janeiro (FAPERJ) [Nos. E-26/204.206/2024 and E-26/211.291/2021], and Conselho Nacional de Desenvlovimento Científico e Tecnológico (CNPq) [No. 305394/2023-1].

References

[1] Dmytro Pesin and Leon Balents. Mott physics and band topology in materials with strong spin-orbit interaction, Nat. Phys. 6 (2010) 376-381.

- [2] Xiangang Wan, Ari M. Turner, Ashvin Vishwanath, and Sergey Y. Savrasov. Topological semimetal and Fermi-arc surface states in the electronic structure of pyrochlore iridates, Phys. Rev. B 83 (2011) 205101.
- [3] Yoshihiko Okamoto, Minoru Nohara, Hiroko Aruga-Katori, and Hidenori Takagi. Spin-Liquid State in the S=1/2 Hyperkagome Antiferromagnet Na₄Ir₃O₈, Phys. Rev. Lett. 99 (2007) 137207.
- [4] Simon Trebst, Ciarán Hickey. Kitaev materials, Phys. Rep. 950 (2022) 1-37.
- [5] Priyanka Thakur, Navdeep Sharma, Dinesh Pathak, Pankaj Sharma, Kamal Kishore, Shashi Dhar and Madan Lal. State-of-art review on smart perovskites materials: properties and applications, Emerg. Mater. 7 (2024) 667-694.
- [6] S. Vasala and M. Karppinen. $A_2B'B''O_6$ perovskites: A review, Prog. Solid State Chem. 43 (2015) 1.
- [7] D. Serrate, J. M. De Teresa, and M. R. Ibarra. Double perovskites with ferromagnetism above room temperature, J. Phys.: Condens. Matter 19 (2007) 023201.
- [8] Y. Krockenberger, K. Mogare, M. Reehuis, M. Tovar, M. Jansen, G. Vaitheeswaran, V. Kanchana, F. Bultmark, A. Delin, F. Wilhelm, A. Rogalev, A. Winkler, and L. Alff. Sr₂CrOsO₆: End point of a spin-polarized metal-insulator transition by 5d band filling, Phys. Rev. B 75 (2007) 020404(R).
- [9] G. Cao, T. F. Qi, L. Li, J. Terzic, S. J. Yuan, L. E. DeLong, G. Murthy, and R. K. Kaul. Novel Magnetism of ${\rm Ir}^{5+}$ (5 d^4) Ions in the Double Perovskite ${\rm Sr}_2{\rm YIrO}_6$, Phys. Rev. Lett. 112 (2014) 056402.
- [10] J. Song, B. Zhao, L. Yin, Y. Qin, J. Zhou, D. Wang, W. Song, and Y. Sun. Reentrant spin glass behavior and magnetodielectric coupling of an Ir-based double perovskite compound, La₂CoIrO₆, Dalton Trans. 46 (2017) 11691.
- [11] L. Bufaiçal, E. Sadrollahi, F. J. Litterst, D. Rigitano, E. Granado, L. T. Coutrim, E. B. Araújo, M. B. Fontes, E. Baggio-Saitovitch, and E. M. Bittar. Effect of structural and magnetic disorder on the 3d-5d exchange interactions in La_{2-x}Ca_xCoIrO₆, Phys. Rev. B 102 (2020) 024436.
- [12] R. D. Shannon. Revised effective ionic radii and systematic studies of interatomic distances in halides and chalcogenides, Acta Cryst. A32 (1976) 751.
- [13] L. T. Coutrim, D. C. Freitas, M. B. Fontes, E. Baggio-Saitovitch, E. M. Bittar, E. Granado, P. G. Pagliuso, L. Bufaiçal. Structural and magnetic properties of the ${\rm La_{2-x}Ca_{x}CoIrO_{6}}$ double perovskite series, J. Solid State Chem. 221 (2015) 373-377.

- [14] N. Narayanan, D. Mikhailova, A. Senyshyn, D. M. Trots, R. Laskowski, P. Blaha, K. Schwarz, H. Fuess, and H. Ehrenberg. Temperature and composition dependence of crystal structures and magnetic and electronic properties of the double perovskites $\text{La}_{2-x}\text{Sr}_x\text{CoIrO}_6$ (0 \leq x \leq 2), Phys. Rev. B 82 (2010) 024403.
- [15] A. Kolchinskaya, P. Komissinskiy, M. B. Yazdi, M. Vafaee, D. Mikhailova, N. Narayanan, H. Ehrenberg, F. Wilhelm, A. Rogalev, and L. Alff. Magnetism and spin-orbit coupling in Ir-based double perovskites $La_{2-x}Sr_xCoIrO_6$, Phys. Rev. B 85 (2012) 224422.
- [16] A. C. Larson and R. B. Von Dreele. General structure analysis system -GSAS/EXPGUI, Los Alamos National Laboratory Report No. LAUR 86-748, 2000; B. H. Toby. EXPGUI, a graphical user interface for GSAS, J. Appl. Crystallogr. 34 (2001) 210.
- [17] J. R. L. Mardegan, L. S. I. Veiga, T. Pohlmann, S. S. Dhesi, S. Francoual, J. R. Jesus, C. Macchiutti, E. M. Bittar, and L. Bufaiçal. 3d and 5d electronic structures and orbital hybridization in Ba- and Ca-doped La₂CoIrO₆ double perovskites, Phys. Rev. B 107 (2023) 214427.
- [18] Mohd Alam and Sandip Chatterjee. B-site order/disorder in $A_2BB'O_6$ and its correlation with their magnetic property, J. Phys.: Condens. Matter 35 (2023) 223001.
- [19] N. W. Ashcroft and N. D. Mermin. Solid State Physics, Cengage Learning, New York (2011).
- [20] B. J. Kim, H. Ohsumi, T. Komesu, S. Sakai, T. Morita, H. Takagi, and T. Arima. Phase-Sensitive Observation of a Spin-Orbital Mott State in Sr₂IrO₄, Science 323 (2009) 1329.
- [21] Kaustuv Manna, R. Sarkar, S. Fuchs, Y. A. Onykiienko, A. K. Bera, G. Aslan Cansever, S. Kamusella, A. Maljuk, C. G. F. Blum, L. T. Corredor, A. U. B. Wolter, S. M. Yusuf, M. Frontzek, L. Keller, M. Iakovleva, E. Vavilova, H.-J. Grafe, V. Kataev, H.-H. Klauss, D. S. Inosov, S. Wurmehl, and B. Büchner. Noncollinear antiferromagnetism of coupled spins and pseudospins in the double perovskite La₂CuIrO₆, Phys. Rev. B 94 (2016) 144437.
- [22] Abhisek Bandyopadhyay, Ilaria Carlomagno, Laura Simonelli, M. Moretti Sala, A. Efimenko, Carlo Meneghini, and Sugata Ray. Evolution of electronic and magnetic properties in a series of iridate double perovskites $\Pr_{2-x} \operatorname{Sr}_x \operatorname{MgIrO}_6$ (x=0,0.5,1.0), Phys. Rev. B 100 (2019) 064416.
- [23] K. C. Kharkwal, Roumita Roy, Harish Kumar, A. K. Bera, S. M. Yusuf, A. K. Shukla, Kranti Kumar, Sudipta Kanungo, and A. K. Pramanik. Structure, magnetism, and electronic properties in 3d-5d based double perovskite $(\operatorname{Sr}_{1-x}\operatorname{Ca}_x)_2\operatorname{FeIrO}_6\ (0\leq x\leq 1)$, Phys. Rev. B 102 (2020) 174401.

- [24] B. Raveau and Md. Motin Seikh, Cobalt Oxides: From Crystal Chemistry to Physics (Wiley-VCH, Weinheim, 2012).
- [25] J. Terzic, H. Zheng, Feng Ye, H. D. Zhao, P. Schlottmann, L. E. De Long, S. J. Yuan, and G. Cao. Evidence for a low-temperature magnetic ground state in double-perovskite iridates with Ir^{5+} (5 d^4) ions, Phys. Rev. B 96 (2017) 064436.
- [26] Klaus K. Wolff, Liu Hao Tjeng, Martin Jansen. The new ordered double perovskite SrLaCuIrO₆, Solid State Commun. 289 (2019) 43-46.
- [27] L. Bufaiçal, L.S.I. Veiga, J.R.L. Mardegan, T. Pohlmann, S. Francoual, S.S. Dhesi, M.B. Fontes, E.M. Bittar. The Co²⁺-Ir⁵⁺ orbital hybridization in LaCaCoIrO₆ double perovskite, J. Magn. Magn. Mater. 587 (2023) 171276.
- [28] Klaus K. Wolff, Stefano Agrestini, Arata Tanaka, Martin Jansen, and Liu Hao Tjeng. Comparative Study of Potentially $J_{eff}=0$ Ground State Iridium(V) in SrLaNiIrO₆, SrLaMgIrO₆, and SrLaZnIrO₆, Z. Anorg. Allg. Chem. 643 (2017) 2095-2101.